Shallow halogen vacancies in halide optoelectronic materials

Hongliang Shi and Mao-Hua Du

Shallow halogen vacancies in halide optoelectronic materials

Hongliang Shi and Mao-Hua Du

Materials Science & Technology Division and Center for Radiation Detection Materials

and Systems, Oak Ridge National Laboratory, Oak Ridge, TN 37831, USA

Halogen vacancies (V_H) are usually deep color centers (F centers) in halides and can act as major electron traps or recombination centers. The deep V_H contributes to the typically poor carrier transport properties in halides. However, several halides have recently emerged as excellent optoelectronic materials, e.g., $CH_3NH_3PbI_3$ and TlBr. Both $CH_3NH_3PbI_3$ and TlBr have been found to have shallow V_H, in contrast to commonly seen deep V_H in halides. In this work, several halide optoelectronic materials, i.e., $CH_3NH_3PbI_3$, $CH_3NH_3SnI_3$ (photovoltaic materials), TlBr, and $CsPbBr_3$, (gamma-ray detection materials) are studied to understand the material chemistry and structure that determine whether V_H is a shallow or deep defect in a halide material. It is found that crystal structure and chemistry of ns^2 ions both play important roles in creating shallow V_H in halides such as $CH_3NH_3PbI_3$, $CH_3NH_3SnI_3$, and TlBr. The key to identifying halides with shallow V_H is to find the right crystal structures and compounds that suppress cation orbital hybridization at V_H, such as those with large cation-cation distances and low anion coordination numbers, and those with crystal symmetry that prevents strong hybridization of cation dangling bond orbitals at V_H. The results of this work provide insight and guidance to identifying halides with shallow V_H as good electronic and optoelectronic materials.

PACS: 61.72.Bb, 61.72.jd, 71.55.Ht

I. Introduction

Halides are usually large-gap ionic materials with low carrier mobilities and soft lattices prone to defect formations. The large band gap and the poor carrier transport properties of many halides have largely prevented them from being used as electronic and optoelectronic materials. Traditionally, halides have been used as optical materials, such as luminescent and scintillation materials.[1, 2, 3, 4] However, recently several halides have been found to be excellent optoelectronic materials. For instances, $CH_3NH_3PbI_3$ based solar cells have achieved impressive energy conversion efficiency of 17.9%.[5, 6] The electron and hole diffusion lengths in $CH_3NH_3PbI_{3-x}Cl_x$ both exceed 1 μm.[7, 8] TlBr, a soft-lattice halide, exhibits excellent transport properties and is being developed as a room-temperature gamma-ray detector material.[9] The electron mobility-lifetime product of TlBr is as high as 6×10^{-3} cm^2/V.[10] The estimated electron lifetime is about 70-100 μs.[9] A number of other halides and chalcohalides, e.g. $CH_3NH_3SnI_3$,[11, 12] $CsSnI_3$,[13] $CsPbBr_3$,[14] Tl_6SeI_4,[15] Tl_6SI_4,[16] etc., have also been shown to exhibit good carrier transport properties. Among these materials, $CH_3NH_3SnI_3$ and $CsSnI_3$ have been proposed as promising photovoltaic materials while $CsPbBr_3$, Tl_6SeI_4, and Tl_6SI_4 are being developed as gamma-ray detection materials.

These halide optoelectronic materials have diverse crystal structures and a wide range of band gap energies. For examples, TlBr, $CH_3NH_3PbI_3$, and $CsPbBr_3$ have simple cubic (*Pm-3m*),[17] body-centered tetragonal (*I4cm*),[18] and orthorhombic (*pnma*)[14] structures at room temperature, and their band gaps are 2.68 eV,[19] 1.51-1.52 eV,[18,20] and 2.25 eV[14], respectively. However, these materials share one common character, i.e., they all have ns^2 cations (i.e., Tl$^+$, Pb^{2+}), which have outermost electron configuration of ns^2.

The halides with ns^2 cations are relatively covalent. The mixed ionic-covalent character of these halides gives rise to enhanced Born effective charges and large static dielectric constant.[21, 22, 23, 24] The ns^2 cations are responsible for the dispersive conduction and valence bands and large dielectric screening of charged defects and impurities,[24] which contribute to the good carrier transport properties in the halides that contain ns^2 cations.

Among these halides with ns^2 cations, TlBr and CH$_3$NH$_3$PbI$_3$ have been extensively investigated and their carrier transport properties are superior compared to many others. Previous defect calculations show that most of the low-energy defects in TlBr and CH$_3$NH$_3$PbI$_3$ are shallow donors or acceptors, which do not introduce deep carrier traps or recombination centers in the band gap. [24, 25, 26, 27] The lack of low-energy deep native defects contribute strongly to the observed excellent transport properties in TlBr and CH$_3$NH$_3$PbI$_3$.

The dominant electron trap in halides is usually the halogen vacancy (V_H), which is typically a deep center (F center) that can cause coloration of many otherwise transparent halide crystals. The F center and the related sub-band-gap optical transitions in alkali halides have been extensively studied for many decades.[28] Even in less ionic halides and chalcohalides (e.g., InI, Tl$_6$SeI$_4$, Tl$_6$SI$_4$) with relatively small band gaps (e.g., 2 eV for InI;[29] 1.86 eV for Tl$_6$SeI$_4$;[15] 2.1 eV for Tl$_6$SI$_4$[16]), V_H^- (with two electrons trapped at a deep level of the halogen vacancy) has been found to be stable when the Fermi level is high in the band gap.[23, 30, 31] It is puzzling why the halogen vacancies in TlBr and CH$_3$NH$_3$PbI$_3$ (with band gaps of 2.68 eV[19] and 1.51-1.52 eV[18,20], respectively) are shallow donors. In light of the outstanding carrier transport properties of TlBr and CH$_3$NH$_3$PbI$_3$ compared to most of other halides, it is important to understand the material

structure and chemistry that determine the shallow or deep nature of V_H in halides. Such understanding is imperative to the discovery and development of new halide-based electronic and optoelectronic materials.

The defect states at V_H are formed by hybridization of dangling bond orbitals from the nearby cations. The lowest defect state at V_H is typically an a_1 state. The occupation of the a_1 state determines the charge state of V_H, i.e., $V_H^+(a_1^0)$, $V_H^0(a_1^1)$, and $V_H^-(a_1^2)$, where a_1^0, a_1^1, and a_1^2 are the a_1 states occupied by zero, one, and two electrons, respectively. At $V_H^+(a_1^0)$, Coulomb repulsion moves the cations away from the vacancy. The resulting weakened dangling bond hybridization leads to a relatively high-lying a_1^0 state. At $V_H^0(a_1^1)$ and $V_H^-(a_1^2)$, the a_1 state is occupied and therefore there is energetic incentive to lower the a_1 state. This is accomplished by relaxation of the nearby cations towards the vacancy, which enhances the hybridization among the cation dangling bond orbitals. The lowering of the a_1 state lowers the electronic energy, which offsets the increased strain energy caused by the stretched bonds near the vacancy.

V_H^0 and V_H^- are F^0 and F^- color centers in large-gap ionic halides. Halides with ns^2 cations are relatively covalent and have relatively small band gaps. In these halides, it is possible that the empty a_1 state of V_H^+ resonates in the conduction band. But V_H^0 and V_H^- can still form because the a_1 state of V_H^0 or V_H^- is lower in energy and can be a bound state inside the band gap. This is the case for InI, Tl_6SeI_4, and Tl_6SI_4, which are discussed in Section III. In this situation, the electron trapping at V_H^+ involves a kinetic barrier because moving the a_1 state of V_H^+ below the CBM before trapping an electron involves moving

nearby cations towards the vacancy, which increases electrostatic energy and strain energy.

Note that V_H^0 and V_H^- in this paper refer to halogen vacancies with one and two electrons trapped at a deep a_1 level not at a shallow hydrogenic level. The thermodynamic transition levels shown in this paper are all for electron trapping at a deep a_1 level.

In low-gap halides, shallow trapping at a hydrogenic level through long-range Coulomb attraction may compete with deep trapping at a localized deep defect state (a_1 state) created by hybridization of cation dangling bond orbitals. Some defects can trap an electron at a deep single-particle a_1 state while the thermodynamic transition level related to the electron trapping is shallow or even above the conduction band minimum (CBM). Note that a thermodynamic defect transition level $\varepsilon(q/q')$ is the Fermi level at which the total energies of the defect at charge states q and q' are equal to each other (defined by Eq. 1 in Section II). A thermodynamic transition level takes into account the structural relaxation upon change of the charge state and thus differs from a single-particle a_1 defect level. If the (+/0) transition level, which is related to electron trapping at a deep a_1 level of a halogen vacancy, is above the CBM, the shallow trapping at a hydrogenic level would be energetically favored and the deep trapping at the a_1 level is metastable. This is the case for Br vacancy in CsPbBr$_3$, as discussed in Section III. In the case of TlBr and CH$_3$NH$_3$PbI$_3$, deep electron trapping at V_H is not even metastable. Electrons instead can only be bound to a V_H at a shallow hydrogenic level through Coulomb attraction.

In this work, V_H in TlBr, CsPbBr$_3$, CH$_3$NH$_3$PbI$_3$ and CH$_3$NH$_3$SnI$_3$ are studied based on density functional calculations. Crystal structure and chemistry of ns^2 ions are

shown to both play important roles in determining the shallow or deep nature of V_H in halides.

II. Methods

Density functional theory (DFT)[32] with both Perdew-Burke-Ernzerhof (PBE)[33] and Heyd-Scuseria-Ernzerhof (HSE) hybrid functional[34] functionals were used to study halogen vacancy properties in halides. The PBE calculations without spin-orbit coupling were used to optimize the structures of the halogen vacancies. If a deep anion vacancy state in the band gap is found by the PBE calculations, the HSE calculations including spin-orbit coupling are further performed to calculate the defect levels. The structures optimized at the PBE level were used for the HSE calculations. The PBE calculations provide sufficiently accurate results on forces (near equilibrium), structures, and band dispersion, but underestimates band gaps. The HSE calculations were performed to correct the band gap and to determine the positions of the deep defect levels relative to valence and conduction band edges. 43% non-local Fock exchange was used in HSE calculations to produce good band gaps. The resulting band gaps of TlBr (simple-cubic CsCl structure), $CH_3NH_3PbI_3$, and $CsPbBr_3$ are 2.74 eV, 1.50 eV, and 2.21 eV, respectively, in good agreement with the experimental values of 2.68 eV,[19] 1.51-1.52 eV,[18,20] and 2.25 eV[14]. The band gap of TlBr with rocksalt NaCl structure is calculated to be 3.08 eV.

The electron-ion interactions were described using projector augmented wave potentials.[35] The valence wavefunctions were expanded in a plane-wave basis with cut-off energies of 400 eV for $CH_3NH_3PbI_3$ and $CH_3NH_3SnI_3$ and 238 eV for $CsPbBr_3$ and

TlBr. All atoms were relaxed to minimize the Feynman-Hellmann forces to below 0.02 eV/Å. All calculations were performed using the VASP codes.[36, 37]

A 64-atom cubic cell and a 2×2×2 k-point mesh were used for RS TlBr. A 2×1×2 orthorhombic supercell containing 16 formula units of $CsPbBr_3$ and a 1×2×1 k-point mesh were used for $CsPbBr_3$. A 3×3×3 tetragonal supercell with 27 formula units of $CH_3NH_3SnI_3$ and a Γ-point-only k-point-mesh were used for $CH_3NH_3SnI_3$. Experimental lattice constants were used for all TlBr (simple-cubic CsCl structure[38] and rocksalt NaCl structure[39]), $CH_3NH_3PbI_3$,[18] $CH_3NH_3SnI_3$,[18] and $CsPbBr_3$[14].

The halogen vacancy formation energy in a halide is a function of the chemical potentials of the constituent elements (μ) and the Fermi level (ε_f): $\Delta H = A(\mu) + q\varepsilon_f$. In this work, the focus is on the charge transition levels induced by the halogen vacancy not the absolute formation energy of the halogen vacancy. Thus, $A(\mu)$ is not explicitly calculated but chosen such that the formation energy of a neutral halogen vacancy is zero. The charge transition level $\varepsilon(q/q')$ for a halogen vacancy is determined by the Fermi level (ε_f) at which the formation energies of the halogen vacancy with charge states q and q' are equal to each other. $\varepsilon(q/q')$ is calculated using

$$\varepsilon(q/q') = (E_{q'} - E_q)/(q' - q), \tag{1}$$

where $E_{q'}$ (E_q) is the total energy of the supercell that contains the relaxed structure of a halogen vacancy at charge state q (q'). The correction to the defect formation energy due to potential alignment (between the host and a charged defect supercell) [40, 41] was applied. We did not apply the image charge correction because experimentally measured static

dielectric constants are not available for all the compounds studied in this paper. However, it is known that the halides with ns^2 cations typically have mixed ionic-covalent character, which leads to strong lattice polarization and large static dielectric constants.[21, 22, 24] Large static dielectric constants (such as 30.6 for TlBr) result in very small image charge corrections,[42] which do not affect the conclusions of this paper.

III. Results and Discussion

A Br vacancy (V_{Br}) in TlBr (simple cubic CsCl structure) has eight neighboring Tl^+ ions. The Tl-Br bond length in TlBr is 3.45 Å. In comparison, the iodine vacancy in Tl_6SeI_4 has fewer Tl^+ neighbors (six) and a longer average Tl-I bond length (3.49 Å). TlBr also has a much larger band gap (2.68 eV)[19] than Tl_6SeI_4 (1.86 eV)[15]. A larger band gap usually favors the formation of deep defects. Nevertheless, V_{Br}^0 and V_{Br}^- in TlBr are unstable whereas, in Tl_6SeI_4, V_I^- is stable when the Fermi level is near the CBM and V_I^0 is metastable.[23] Therefore, the size of the anion vacancy, the anion coordination number, and the band gap are unlikely the important factors that lead to the shallow V_{Br} in TlBr.

The V_{Br} defect state in TlBr is derived from the conduction band states which have predominantly the Tl-6p characters. Figure 1 shows the partial charge density of the CBM state, which clearly exhibits the directional Tl-6p characters. The lobes of the Tl-6p orbitals point at the nearest-neighbor Tl ions instead of the nearest neighbor Br ions because the symmetry of the p orbitals is compatible with the symmetry of the Tl sublattice which has the six fold coordination for Tl. This leads to relatively weak Tl-Br hybridization and long Tl-Br bond length in TlBr. In V_{Br}, there is not sufficient

hybridization among the Tl-6p orbitals to form a bonding orbital due to the relatively large distance between the center of the Br vacancy and the surrounding Tl cations.
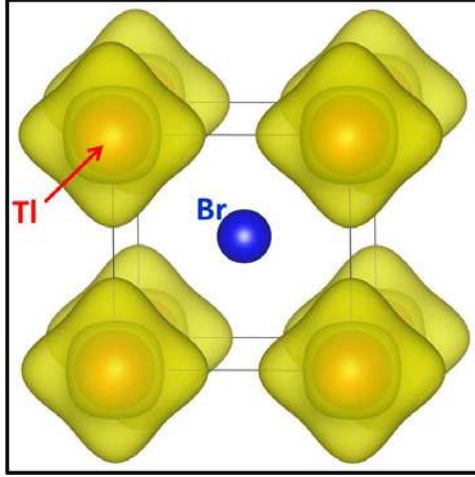

Figure 1. **Charge density contour (yellow isodensity surface) of the CBM state in SC TlBr. The red and blue balls represent Tl and Br ions respectively.**

To gain more insight, V_{Br} in TlBr of rock-salt (RS) NaCl structure is studied. TlBr has a simple cubic (SC) CsCl structure at room temperature. RS TlBr has been synthesized by surface deposition at low temperatures.[39] In RS TlBr, every Tl^+ cation is bonded with six Br^- anions. The Tl-6p and Br-4p orbitals in RS TlBr point at each other and have better orbital overlap than in SC TlBr. The resulting Tl-Br bond in RS TlBr is more covalent with a bond length of 3.30 Å, shorter than that in SC TlBr, which is 3.45 Å. V_{Br} in RS TlBr is found to be a deep F center by hybrid density functional calculations. Figure 2 shows the formation energies of V_{Br}^+, V_{Br}^0 and V_{Br}^- in RS TlBr. The (+,0), (0/-), and (+/-) charge transition levels, calculated using Eq. 1 are all located inside the band gap. At V_{Br}, six Tl 6p orbitals point at the center of the Br vacancy, forming a bound a_1 state, as shown, for example, for V_{Br}^- in Figure 3. The a_1 states of V_{Br}^+ and V_{Br}^- are

0.14 eV and 0.75 eV below the CBM, respectively. For V_{Br}^0, the half-occupied a_1 state is split to a lower-lying occupied state and a higher-lying empty state, which are 1.05 eV and 0.23 eV below the CBM, respectively. The Tl-Tl distances at V_{Br}^+, V_{Br}^0, and V_{Br}^- are 6.80 Å, 6.22 Å, and 5.78 Å. In comparison, the Tl-Tl distance is 6.59 Å in the absence of V_{Br}. Clearly, the electron trapping at the a_1 state of V_{Br} is accompanied by strong relaxation of Tl cations towards the center of the vacancy.

The comparison between Br vacancies in SC and RS TlBr suggests that the special chemistry of the ns^2 ion (which gives rise to p-orbital derived conduction band states) and the crystal structure both play important roles in creating shallow V_{Br} in SC TlBr. In halides that contain ns^2 cations, the hybridization strength of the cation-p orbitals, which are directional, in a halogen vacancy strongly depends on the crystal structure. When the symmetry of the crystal structure prevents the cation p orbitals from pointing towards the nearest-neighbor halogen anions as is the case for SC TlBr, the cation-anion distance would be relatively long and the hybridization between the cation-p orbitals in the halogen vacancy could be substantially reduced to cause the absence of the vacancy-induced bound defect state in the band gap. In contrast, the conduction band of alkali halides is made up of cation-s orbitals. These cation-s orbitals have spherical symmetry and can hybridize to form an s-like bound state in a halogen vacancy in alkali halides of both RS and SC structure.[43]
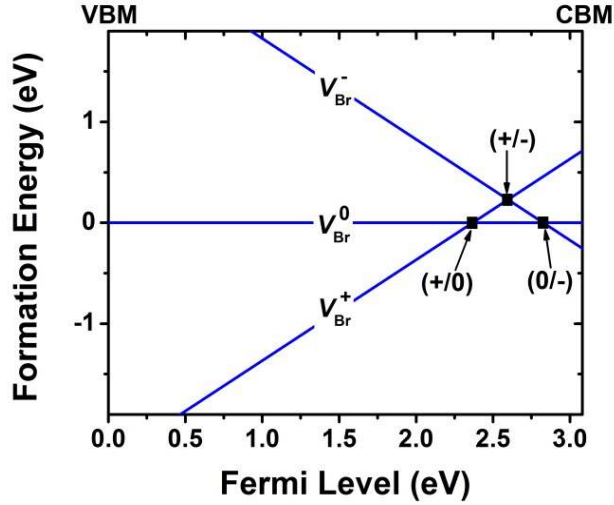
Figure 2. **Formation energies of V_{Br} at +1, neutral, and -1 charge states in RS TlBr. The formation energy of the neutral V_{Br} is set to zero. The transition level $\varepsilon(q/q')$ [i.e, (+/0), (0/-), and (+/-) levels] is the Fermi level, at which the two formation energy lines with charge states q and q' cross. The valence band maximum (VBM) and the CBM are at zero and 3.08 eV, respectively.**
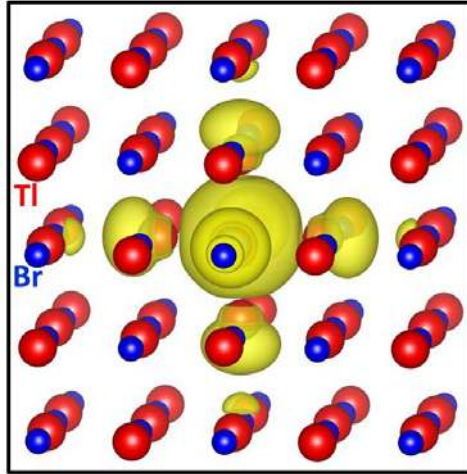

Figure 3. **Charge density contour (yellow isodensity surface) of the occupied a_1 state of V_{Br}^- in the band gap of RS TlBr. The red and blue balls represent Tl and Br ions respectively.**

CH₃NH₃PbI₃ has a distorted ABX₃ perovskite structure (body-centered tetragonal structure; space group I4cm) at room temperature.[18] Each Pb^{2+} cation is bonded to six iodine ions. The Pb-6p and the I-5p orbitals point towards each other forming strong

covalent bonds. Nevertheless, the iodine vacancy in $CH_3NH_3PbI_3$ is a shallow donor. This is likely related to the low coordination number (i.e., 2) for iodine anions. In an iodine vacancy, although the Pb-6p orbitals of the nearby Pb^{2+} cations point directly at the center of the vacancy, there are only two Pb-6p orbitals involved in the hybridization. In addition, the large A-site ion, $(CH_3NH_3)^+$, increases the lattice constant and the Pb-Pb distance, which further weaken the hybridization between the Pb-6p orbitals in an iodine vacancy. Therefore, the few number of Pb^{2+} neighbors and the large $(CH_3NH_3)^+$ ions may result in the weak hybridization of Pb-6p orbitals in the iodine vacancy (V_I), which is insufficient to lower the a_1 defect level below the CBM to create a bound state. To prove this point, V_{Br} in $CsPbBr_3$ is studied. $CsPbBr_3$ has a smaller A-site cation and a smaller halogen anion than those in $CH_3NH_3PbI_3$, which should decrease the Pb-Pb distance and consequently enhance the hybridization of Pb 6p orbitals in the Br vacancy.

$CsPbBr_3$ is a promising room-temperature gamma ray detection material.[14] It has a distorted perovskite structure (orthorhombic structure; space group *pnma*).[14] There are two inequivalent Br sites in $CsPbBr_3$, i.e., equatorial and epical sites. V_{Br}^+ and V_{Br}^- on the equatorial site are calculated to be more stable than those on the apical site by 0.13 eV and 0.40 eV, respectively, at the PBE level, consistent with the trend in $CH_3NH_3PbI_3$. Thus, V_{Br} in $CsPbBr_3$ thereafter refers to V_{Br} on the equatorial site.

The Pb-Pb distance in V_{Br}^+ in $CsPbBr_3$ is calculated to be 5.99 Å, which is much shorter than that in V_I^+ in $CH_3NH_3PbI_3$ (6.58 Å). V_I in $CH_3NH_3PbI_3$ does not form a bound a_1 state in the band gap. But V_{Br} in $CsPbBr_3$ is found to be capable of localizing one or two electrons accompanied by strong structural relaxation (shortening of the Pb-Pb distance). The calculated Pb-Pb distances at V_{Br}^+, V_{Br}^0, and V_{Br}^- in $CsPbBr_3$ are 5.99 Å, 5.15

12

Å, and 3.70 Å, respectively. In comparison, the Pb-Pb distance is 5.82 Å in the absence of V_{Br}. The empty a_1 defect state of V_{Br}^+ is above the CBM. The fully occupied a_1 state of V_{Br}^- is 0.80 eV below the CBM. For V_{Br}^0, the half-occupied a_1 state is split to a lower-lying occupied state, which is 0.46 eV below the CBM, and a higher-lying empty state, which is above the CBM. The partial charge density of the bound a_1 state of V_{Br}^- is shown in Figure 4. At V_{Br}^-, the strong Pb-6p hybridization creates a fully occupied strongly bound state. The lowered electronic energy offsets the strain energy induced by the shortening of the Pb-Pb distance.
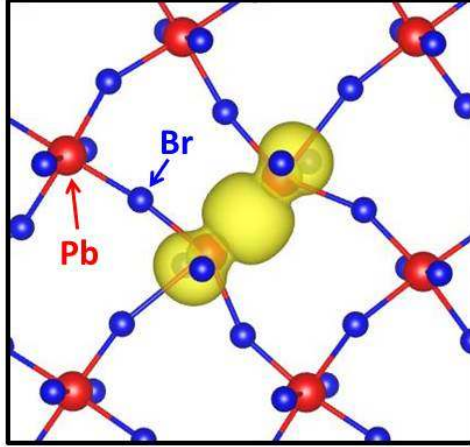

Figure 4. **Charge density contour (yellow isodensity surface) of occupied bound defect state for V_{Br}^- in CsPbBr$_3$. Only one layer of corner-shared PbBr$_6$ octahedra is shown and Cs ions are not shown for clarity. The red and blue balls represent Pb and Br ions respectively.**

Figure 5 shows the calculated formation energies of V_{Br}^+, V_{Br}^0, and V_{Br}^- in CsPbBr$_3$. The (+/-) transition level is 0.05 eV below the CBM. So V_{Br}^- is stable when the Fermi level is near the CBM. The (+/0) and the (0/-) transition levels are calculated to be 0.16 eV above the CBM and 0.26 eV below the CBM, respectively. V_{Br}^0 is metastable as shown in Fig. 5. Therefore, V_{Br} in CsPbBr$_3$ is a negative-U center. This is the result of strong

structural relaxation upon trapping electrons. In high-resistivity $CsPbBr_3$ (high resistivity is required for semiconductor radiation detection materials.[44,45]), the Fermi level is near the midgap and V_{Br}^+ is stable. Since the (+/0) transition level is above the CBM (Figure 5), V_{Br}^0 with a deep bound state is less stable than the neutral hydrogenic center and thus the electron should be trapped by V_{Br}^+ at a shallow hydrogenic level. This is consistent with the reported good electron mobility and lifetime in high-resistivity $CsPbBr_3$.[14]
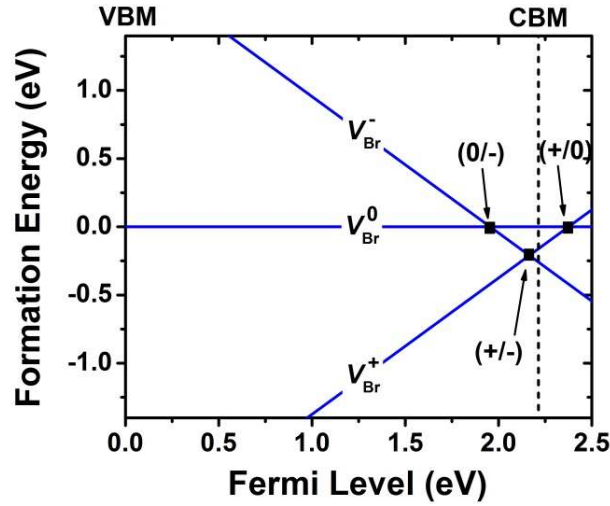

Figure 5. **Formation energies of V_{Br} at +1, neutral, and -1 charge states in CsPbBr$_3$. The formation energy of the neutral V_{Br} is set to zero. The transition level $\varepsilon(q/q')$ [i.e., (+/0), (0/-), and (+/-) levels] is the Fermi level, at which the two formation energy lines with charge states q and q' cross. The valence band maximum (VBM) and the CBM are at zero and 2.21 eV, respectively.**

Different hybridization strengths of Pb-6p orbitals result in the different electronic properties of the halogen vacancies in $CH_3NH_3PbI_3$ and $CsPbBr_3$. Note that the larger $CsPbBr_3$ band gap than that of $CH_3NH_3PbI_3$ is not the reason for the different halogen vacancy properties in these two halides because the band gap difference is mainly due to the lower Br-4p-derived valence band in $CsPbBr_3$ than I-5p-derived valence band in

CH$_3$NH$_3$PbI$_3$. The conduction bands of these two halides are both made up of mainly Pb-6p states, from which the halogen vacancy state is derived.

CH$_3$NH$_3$SnI$_3$ is a recently investigated photovoltaic material. Compared to V_I in CH$_3$NH$_3$PbI$_3$, which is already a shallow donor, the Sn-5p orbitals around V_I in CH$_3$NH$_3$SnI$_3$ are spatially less extended than the Pb-6p orbitals in CH$_3$NH$_3$PbI$_3$ and thus are more difficult to hybridize to form a bound state in the band gap. Indeed, V_I in CH$_3$NH$_3$SnI$_3$ is found to be a shallow donor by density functional calculations. V_I^+ cannot localize electrons to form deep centers.

In addition to TlBr, there are several halides/chalcohalides (e.g., InI, Tl$_6$SeI$_4$, and Tl$_6$SI$_4$) that have been studied recently for their potential radiation detection applications. The (+/-), (+/0), and (0/-) transition levels of V_I in InI and Tl$_6$SeI$_4$ are all inside the band gap.[23, 30, 31] The iodine coordination numbers in InI, Tl$_6$SeI$_4$, and Tl$_6$SI$_4$ are five, six, and six, respectively, compared to two in perovskite halides (i.e., CH$_3$NH$_3$PbI$_3$, CH$_3$NH$_3$SnI$_3$ and CsPbBr$_3$). The local symmetries around the iodine vacancies in InI, Tl$_6$SeI$_4$, and Tl$_6$SI$_4$ are low and do not prevent the hybridization of the Tl-6p orbitals at vacancies. Therefore, the a_1 states of V_I^0 and V_I^- in InI, Tl$_6$SeI$_4$, and Tl$_6$SI$_4$ are bound states inside the band gap. Although the (+/0) transition level is below the CBM, the electron trapping at V_I^+ should involve a kinetic barrier because the a_1 defect state of V_I^+ is above the CBM. (The thermodynamic (+/0) transition level is inside the band gap because of the large structural relaxation upon the electron trapping.) This should reduce the electron trapping cross-section at V_I^+ in these materials.

Based on the electron trapping properties of the positively charged halogen vacancy (V_H^+), halides can be categorized into four groups. In the first group, only V_H^+ is

stable and deep trapping is not even metastable. (In other words, V_H^+ cannot localize electrons at a deep level.) TlBr, $CH_3NH_3PbI_3$, and $CH_3NH_3SnI_3$ belong to this group. In the second group, V_H^+ is capable to localize one or two electrons at a deep a_1 defect state to form V_H^0 and V_H^-. The (+/-) transition level is inside the band gap but the (+/0) transition level is above the CBM (negative-U character). Therefore, deep electron trapping at V_H^+ is energetically unfavorable compared to trapping at a hydrogenic shallow level. $CsPbBr_3$ belongs to this group. In the third group, electron trapping at a deep (+/0) level of the halogen vacancy is energetically favorable but is subject to a kinetic barrier (because the a_1 level of V_H^+ is above the CBM). InI, Tl_6SeI_4, and Tl_6SI_4 belong to this group.[23,30] Most of the large-gap ionic halides (such as alkali halides) belong to the fourth group, in which electrons can be deeply trapped at the halogen vacancy with no appreciable kinetic barrier. (The thermodynamic transition levels and the single-particle a_1 levels of the halogen vacancy are all inside the band gap.) These materials may be used as optical materials like scintillators but usually not as electronic or optoelectronic materials.[4,46]

V. Conclusions

In light of the exceptionally good carrier transport efficiency in several halide optoelectronic materials (e.g., $CH_3NH_3PbI_3$ and TlBr) and its correlation with the lack of halogen vacancy induced deep electron traps, we performed density functional calculations to understand the material structure and chemistry that create shallow halogen vacancies in these halides. The halogen vacancies in TlBr and $CsPbBr_3$, two promising room-temperature gamma-ray detector materials, and $CH_3NH_3PbI_3$ and $CH_3NH_3SnI_3$, two high-performance photovoltaic materials, are studied in details. The

shallow-donor nature of halogen vacancies in $CH_3NH_3PbI_3$ and TlBr is explained by the insufficient hybridization among cation orbitals around the halogen vacancy, which is related to the crystal structure and the chemistry of ns^2 ions in these halides. We further predict that the iodine vacancy in $CH_3NH_3SnI_3$ is also a shallow donor. For $CsPbBr_3$, our calculations show that, although V_{Br}^- (which has two electrons trapped at V_{Br}) is stable when the Fermi level is near the CBM, the trapping of one electron at V_{Br}^+ (which is stable in $CsPbBr_3$ radiation detector where the Fermi level is near midgap) should occur at a shallow hydrogenic level. These results suggest that shallow halogen vacancies can exist in halides to give rise to good carrier transport properties. The key is to find the right crystal structures and compounds, such as those with large cation-cation distances and low anion coordination numbers, and those with crystal symmetry that prevents strong hybridization among cation orbitals in the halogen vacancy.

Acknowledgements

[1] G. Blasse and B. C. Grabmaier, "Luminescent Materials", Springer-Verlag, Berlin (1994).

[2] P. A. Rodnyi, "Physical Processes in inorganic scintillators", CRC Press, Boca Raton (1997).

[3] J. B. Birks, "The theory and practice of scintillation counting", Pergamon Press Ltd. (1964).

[4] M. H. Du, J. Mater. Chem. C **2**, 4784 (2014**)**.

[5] https://www.nrel.gov/ncpv/images/efficiency_chart.jpg.

[6] M. A. Green, A. Ho-Baillie, and H. J. Snaith, Nature Photonics **8**, 506 (2014**)**.

[7] S. D. Stranks, G. E. Eperon, G. Grancini, C. Menelaou, M. J. Alcocer, T. Leijtens, L. M. Herz, A. Petrozza, and H. J. Snaith, Science **342**, 341 (2013**)**.

[8] G. Xing, N. Mathews, S. Sun, S. S. Lim, Y. M. Lam, M. Grätzel, S. Mhaisalkar, T. C. Sum, Science **342**, 344 (2013**)**.

[9] A. V. Churilov, C. Ciampi, H. Kim, L. J. Cirignano, W. M. Higgins, F. Olschner, and K. S. Shah IEEE Trans. Nucl. Sci. **56**, 1875 (2009).

[10] A. V. Churilov, C. Ciampi, H. Kim, W. M. Higgins, L. J. Cirignano, F. Olschner, V. Biteman, M. Minchello, and K. S. Shah, J. Cryst. Growth **312**, 1221 (2010).

[11] F. Hao, C. C. Stoumpos, D. H. Cao, R. P. H. Chang, M. G. Kanatzidis, Nature Photonics **8**, 489 (2014).

[12] N. K. Noel, S. D. Stranks, A. Abate, C. Wehrenfennig, S. Guarnera, A. Haghighirad, A. Sadhanala, G. E. Eperon, S. K. Pathak, M. B. Johnston, A. Petrozza, L. M. Herz, and H. J. Snaith, Energy Environ. Sci. DOI: 10.1039/c4ee01076k.

[13] I. Chung, B. Lee, J. He, R. P. H. Chang, and M. G. Kanatzidis, Nature **485**, 486 (2012).

[14] C. C. Stoumpos, C. D. Malliakas, J. A. Peters, Z. Liu, M. Sebastian, J. Im, T. C. Chasapis, A. C. Wibowo, D. Y. Chung, A. J. Freeman, B. W. Wessels, and M. G. Kanatzidis, Cryst. Growth Design **13**, 2722 (2013).

[15] S. Johnsen, Z. Liu, J. A. Peters, J. –H. Song, S. Nguyen, C. D. Malliakas, H. Jin, A. J. Freeman, B. W. Wessels, and M. G. Kanatzidis, J. Am. Chem. Soc. **133**, 10030 (2011)**.**

[16] S. L. Nguyen, C. D. Malliakas, J. A. Peters, Z. Liu, J. Im, L. –D. Zhao, M. Sebastian, H. Jin, H. Li, S. Johnsen, B. W. Wessels, A. J. Freeman, M. G. Kanatzidis, Chem. Mater. **25**, 2868 (2013).

[17] A. Smakula, J. Kalnajs, Phys. Rev. **99**, 1737 (1955).

[18] C. C. Stoumpos, C. D. Malliakas, and M. G. Kanatzidis, Inorg. Chem. **52**, 9019 (2013).

[19] A. Owens and A. Peacock, Nucl. Instru. Methods Phys. Res. A **531**, 18 (2004).

[20] T. Baikie, Y. Fang, J. M. Kadro, M. Schreyer, F. Wei, S. G. Mhaisalkar, M. Grätzel, and T. J. White, J. Mater. Chem. A **1**, 5628 (2013).

[21] M. H. Du, and D. J. Singh, Phys. Rev. B **81**, 144114 (2010).

[22] M. H. Du, and D. J. Singh, Phys. Rev. B **82**, 045203 (2010).

[23] K. Biswas, M. H. Du, and D. J. Singh, Phys. Rev. B **86**, 144108 (2012).

[24] M. H. Du, J. Mater. Chem. A **2**, 9091 (2014).

[25] M. H. Du, J. Appl. Phys. **108**, 053506 (2010).

[26] W. J. Yin, T. Shi, and F. F. Yan, Appl. Phys. Lett. **104**, 063903 (2014).

[27] W. J. Yin, T. T. Shi, and Y. F. Yan, Adv. Mater. **26**, 4653 (2014).

[28] J. H. Schulman and W. D. Compton, "Color centers in solids", Oxford, Pergamon (1962).

[29] R. Farrell, F. Olschner, K. Shah, and M. R. Squillante, Nucl. Instrum. Meth. Phys. Res. A **387**, 194 (1997).

[30] K. Biswas and M. H. Du, J. Appl. Phys. **109**, 113518 (2011).

[31] H. Shi and M. H. Du, unpublished.

[32] W. Kohn and L. J. Sham, Phys. Rev. **140**, A1133 (1965).

[33] J. P. Perdew, K. Burke, and M. Ernzerhof, Phys. Rev. Lett. **77**, 3865 (1996).

[34] J. Heyd, G. E. Scuseria, and M. Ernzerhof, J. Chem. Phys. **125**, 224106 (2006).

[35] P. E. Blöchl, Phys. Rev. B 50, 17953 (**1994**).

[36] G. Kresse and J. Furthmüller, Phys. Rev. B 54, 11169 (**1996**).

[37] G. Kresse and D. Joubert, Phys. Rev. B **59**, 1758 (1999).

[38] M. A. Popova, T. J. Darvojd, M. A. Gurevich, Zhurnal Neorganicheskoi Khimii **11**, 1236 (1966).

[39] M. Blackman and I. H. Khan Proc. Phys. Soc. **77**, 471 (1961).

[40] S. Lany and A. Zunger, Phys. Rev. B **78**, 235104 (2008).

[41] C. G. Van de Walle and J. Neugebauer, J. Appl. Phys. **95**, 3851 (2004).

[42] M. H. Du, Appl. Phys. Lett. 102, 082102 (2013).

[43] A. I. Popov and E. Balanzat Nucl. Instr. Meth. Phys. Res. B **166-167**, 545 (2000).

[44] M. H. Du, H. Takenaka, and D. J. Singh, Phys. Rev. B **77**, 094122 (2008).

[45] K. Biswas and M. H. Du, New J. Phys. **14**, 063020 (2012).

[46] M. H. Du, J. Appl. Phys. **112**, 123516 (2012).